



B3Y-FETAL effective interaction in the folding analysis of elastic scattering of $^{16}\text{O} + ^{16}\text{O}$

I. Ochala¹ · J. O. Fiase²

Received: 16 December 2020 / Revised: 25 May 2021 / Accepted: 26 May 2021 / Published online: 5 August 2021

© China Science Publishing & Media Ltd. (Science Press), Shanghai Institute of Applied Physics, the Chinese Academy of Sciences, Chinese Nuclear Society 2021

Abstract In this paper, a new M3Y-type effective nucleon–nucleon interaction, derived based on the lowest order constrained variational approach (LOCV) and termed B3Y-Fetal, has been used in DDM3Y1, BDM3Y1, BDM3Y2, and BDM3Y3 density-dependent versions in a heavy ion (HI) optical potential based on four types of a real folded potential and a phenomenological Woods–Saxon imaginary potential to study the elastic scattering of the $^{16}\text{O}+^{16}\text{O}$ nuclear system within the framework of the optical model (OM) by computing the associated differential cross sections at various incident energies. The results of the folding analyses have shown the DDB3Y1-Fetal and BDB3Y1-Fetal, out of the four folded potentials, give a reasonably better description of the elastic data of the nuclear system. These best-fit folded potentials are followed, in performance, by the BDB3Y2-Fetal, with the BDB3Y3-Fetal potential coming last. This performance trend was also demonstrated by the optical potentials based on the M3Y-Reid interaction. Furthermore, the best-fit folded potentials, renormalized by a factor N_R of approximately 0.9, have been shown to reproduce the energy dependence of the real optical potential for ^{16}O scattering found in previous optical model analyses creditably well. In excellent agreement with previous works, they have also been identified in this work to belong to the family of deep refractive potentials because they have been able to

reproduce and consistently describe the evolution of Airy-like structures, at large scattering angles, observed in the ^{16}O scattering data at different energies. Finally, a comparison of the performances of B3Y-Fetal and M3Y-Reid effective interactions undertaken in this work has shown impressive agreement between them.

Keywords B3Y-Fetal · Folding analysis · Elastic scattering · Optical model · Incident energies

1 Introduction

The folding model is a microscopic optical potential that has been developed to meet the need for an optical model (OM) to give a unified description of nucleon–nucleon, nucleon–nucleus and nucleus–nucleus scattering [1]. For years, it has been used to calculate the elastic potential for heavy ions and the inelastic form factor [2]. It is believed to be the first-order term of the optical potential derived from Feshbach’s theory of nuclear reactions [3, 4], and it generates the real parts of both nucleon–nucleus and nucleus–nucleus potentials [5, 6]. Its remarkable success in describing the observed elastic scattering in many systems shows that it produces the dominant part of the real optical potential.

In this work, we use a newer approach in OM analysis, in which the optical potential is derived in the framework of macroscopic approximation using nuclear matter properties, nuclear surface, density distributions of nuclei, and an effective interaction. Here, the nuclear matter properties are incorporated in the OM analysis through the use of the double folding model [3]. In this approach, the optical potential is generated by folding an effective nucleon–

✉ I. Ochala
ojoagbamiisaiah1234@gmail.com

¹ Department of Physics, Kogi State University,
P.M.B 1008 Anyigba, Nigeria

² Department of Physics, Benue State University, Makurdi,
Nigeria

nucleon (NN) interaction over the ground-state density distributions of the two nuclei [1, 7]. Of all effective interactions, the M3Y-type interaction, which is based on a realistic NN force, is a popular choice for use in the double folding model [8, 9]. Consequently, different density-dependent versions of the M3Y-Reid and M3Y-Paris interactions designed within the Hartree–Fock (HF) formalism that generate different values of the incompressibility, K , of nuclear matter, have been severally used either in the single-folding [4] or double-folding models [2, 7]. In the same vein, the new M3Y-type effective interaction, derived by Fiase and co-researchers [10] and based on the lowest order constrained variational approach (LOCV), called B3Y-Fetal [11] for the purpose of identification, has been successfully applied to nuclear matter calculations with values of incompressibility K that have been found to demonstrate excellent agreement with previous work with the M3Y-Reid and M3Y-Paris interactions.

The new effective interaction is used herein in its DDM3Y and BDM3Y density-dependent versions to perform a detailed analysis of the refractive nucleus–nucleus scattering of a nuclear system. The B3Y-Fetal is used alongside the M3Y-Reid interaction in the DDM3Y1, BDM3Y1, BDM3Y2, and BDM3Y3 versions for the folding analysis following the approach of Khoa et al. [7, 8] with the intent to determine and compare the performance of the first with the second interaction. To reproduce the empirical energy dependence of the nucleon–nucleus optical potential, a weak intrinsic energy dependence is introduced into the new effective interaction. Because the energy dependence of the real optical potential comes mostly from the exchange term [7], the study of the elastic scattering of chosen light heavy ions is carried out in this work at various collision energies of interest using the exact finite-range evaluation of the exchange potential by means of local approximation within the context of the double folding model. This approach has been used with immense success by many researchers [12]. Because the nuclear system considered here is spin-saturated, only the isoscalar component of the new M3Y-type effective interaction is chiefly employed in all optical model analyses. The folded potential arising from the double folding model is useful only for the real part of the optical potential, and it is supplemented by a phenomenological imaginary part [13].

The choice of the nuclear system for this study is based on reasons related directly to its peculiarities, one of which is that it exhibits weak absorption in elastic scattering so that refractive scattering occurs in it. The refractive scattering in this system is known to provide important information on the equation of state (EOS) of nuclear matter [2, 7] because the double folding model, with an effective NN interaction appropriately adjusted to nuclear matter

properties, enters the optical model analyses as a mean-field effect that produces a very deep real component of the optical potential for the elastic channel. In this way, analysis of the chosen system provides a unique opportunity to gain clear insight into the nature of the EOS of normal nuclear matter. Furthermore, refractive scattering in this system plays a great role in the determination of the real component of the heavy-ion (HI) optical potential down to small inter-nuclear distances, giving the possibility of testing various theoretical models [2, 14] for HI optical potential. Because B3Y-Fetal is an effective interaction based on a theoretical model, different from the theoretical models for other effective interactions that are popularly used for constructing HI optical potentials, it is strongly believed that the study of the elastic scattering of the chosen light heavy ions, using a HI optical potential derived from the new effective interaction, affords ample opportunity to test and affirm the theoretical model used for developing the effective interaction.

In view of the foregoing, we are determined to apply the newly developed B3Y-Fetal interaction to the folding analysis of the chosen light heavy ions within the framework of the OM in the present work, in anticipation that the expected results will provide insight into those qualities that will help determine the true place of the new effective interaction among the numerous theoretical models for HI optical potential. It is also hoped that the data arising from the nuclear reactions will give a clear picture of the EOS of nuclear matter, the nuclear reaction dynamics of the nuclear systems involved, and the relative performance of the effective interactions used. In this light, the remainder of this paper is organized as follows. Section 2 provides an overview of the density- and energy-dependent B3Y-Fetal interactions. In Sect. 3, explanation of the basic features of the double folding model employed for the study of nuclear reactions is provided. In Sect. 4, we present the results of our calculated cross sections and compare them with experimental data, while Sect. 5 focusses on summary and discussion.

2 Density- and energy-dependent B3Y-Fetal interaction

The B3Y-Fetal interaction is a variational effective interaction derived from the lowest order constrained variational approach [10]. The matrix elements were calculated using a harmonic oscillator basis, and the details of the calculation were reported in [10] and in our earlier report, in which we applied it to symmetric nuclear matter (SNM) calculations [11]. In this study, we use the isoscalar part of the B3Y-Fetal effective interaction [10], whose

Table 1 Yukawa strengths of the central components of B3Y-Fetal and M3Y-Reid interactions

Interaction	<i>i</i>	1/ μ_i (fm)	γ^D (MeV)	γ^{EX} (MeV)
B3Y-Fetal	1	0.25	10472.13	499.63
	2	0.40	− 2203.11	− 1347.77
	3	1.414	0.0	− 7.8474
M3Y-Reid	1	0.25	7999.00	4631.375
	2	0.40	− 2134.25	− 1787.125
	3	1.414	0.0	− 7.8474

Yukawa strengths (in MeV) are given in Table 1 along with those of the M3Y-Reid [15]:

Here, the radial shape of the isoscalar M3Y-type effective interaction is expressed in terms of three Yukawas as [15]:

$$v^{D(EX)}(r) = \sum_{i=1}^3 Y^{D(EX)}(i) \frac{\exp(-\mu_i r)}{\mu_i r}, \tag{1}$$

where the functions $Y^{D(EX)}$ are represented in terms of the singlet even (SE), singlet odd (SO), triplet even (TE), and triplet odd (TO) angular momenta channels [15]. To be able to reproduce the saturation properties of cold symmetric nuclear matter and satisfy the requirement for folding analysis, the B3Y-Fetal interaction is used in the energy- and density-dependent form [12, 16]:

$$v^{D(EX)}(E, \rho, r) = g(E)h(\rho)v^{D(EX)}(r), \tag{2}$$

where $h(\rho)$ is the density-dependent factor and $g(E) \simeq 1 - 0.002E$ for M3Y-Reid [7, 8] as well as B3Y-Fetal; E is the incident nucleon energy. This isoscalar energy- and density-dependent interaction has been tested and found to work well in folding model analyses of refractive α -nucleus [8] and nucleus–nucleus [8] elastic scattering. The explicit forms of $h(\rho)$ used in this study are [7, 8]:

$$h(\rho) = C(1 + ye^{-z\rho}) \tag{3}$$

for the DDM3Y $_n$ ($n = 1$) interaction and

$$h(\rho) = C(1 - y\rho^z) \tag{4}$$

for the BDM3Y $_n$ ($n = 0, 1, 2, 3$) interactions. The parameters C , y , and z of the density dependences are such that they reproduce the saturation properties of nuclear matter at density $\rho_0 = 0.17 \text{ fm}^{-3}$, with a binding energy of $E/A = 16 \text{ MeV}$ within HF calculations.

To ascertain the functional viability of the B3Y-Fetal interaction, we applied it to symmetric nuclear matter studies in [11] in its DDM3Y $_n$ and BDM3Y $_n$ density-

dependent versions and found it to demonstrate excellent agreement with both the M3Y-Reid and M3Y-Paris interactions. The curves of the EOS of cold symmetric nuclear matter obtained with the DDB3Y1-, BDB3Y0-, BDB3Y1-, BDB3Y2-, and BDB3Y3-Fetal interactions, found to have incompressibility values $K_0 = 176, 196, 235, 351,$ and 467 MeV , respectively, were well illustrated in [11]. Each of these interactions has been found to reproduce the saturation of nuclear matter at density $\rho = 0.17 \text{ fm}^{-3}$ and binding energy per nucleon $\frac{E}{A} = 16 \text{ MeV}$ correctly, demonstrating good agreement with the work of [12], which is a good basis for certainty and confidence that B3Y-Fetal will perform well in folding analyses. Importantly, DDB3Y1-, BDB3Y0-, BDB3Y1-, BDB3Y2-, and BDB3Y3-Fetal interactions and their corresponding K -values are known to distinguish different nuclear EOSs in nuclear reactions and provide vital information on the nuclear matter EOS. In particular, the DDM3Y1 and BDM3Y1 versions of the B3Y-Fetal used in this work, the most realistic interactions, have given for SNM at equilibrium incompressibility $K_0 \simeq 176\text{--}235 \text{ MeV}$, and this compares favorably well with $K_0 \simeq 171\text{--}232 \text{ MeV}$ and $K_0 \simeq 176\text{--}270 \text{ MeV}$ predicted by the same versions of the M3Y-Reid and M3Y-Paris effective interactions, respectively, in [12]. When this is compared with the experimental estimate of $K_0 = 200\text{--}350 \text{ MeV}$ based on studies on giant monopole resonances [17] and the theoretical estimates of $K_0 = 220 \pm 50 \text{ MeV}$ and $K_0 \simeq 250\text{--}270 \text{ MeV}$ [12], based on non-relativistic and relativistic mean-field models, respectively [18], for SNM, it is evident that the prediction of the B3Y-Fetal interaction is in good agreement. It is with this strong and positive expectation that we use it in the optical model analyses in this paper.

For the folding calculation in this paper, the isoscalar component of the density- and energy-dependent B3Y-Fetal interaction is chiefly employed in all optical model analyses, based on the fact that the system considered involves spin-saturated nuclei. Specifically, the B3Y-Fetal is used in its DDM3Y1, BDM3Y1, BDM3Y2, and BDM3Y3 versions, along with the M3Y-Reid interaction, for folding analysis following the approach of Khoa et al. [7, 8], with the intent of determining and comparing the performance of the first with the second interaction.

3 B3Y-Fetal in folding analysis

The double folding model is a well-established theory and computational procedure that provides an adequate description of the average properties of nucleus–nucleus scattering. In this model, the direct and exchange parts of the nucleus–nucleus potential are obtained by folding the

densities of the projectile and target nuclei with the direct and exchange components of the effective NN interaction in Eq. (2). Thus, the resulting optical potential is

$$V_F(E, R) = V_D(E, R) + V_{EX}(E, R), \quad (5)$$

where $V_D(E, R)$ and $V_{EX}(E, R)$ are the direct and exchange components of the real folded potential, respectively, shown explicitly in [7, 12].

The direct component of the folded potential is local in coordinate space, but the exchange is non-local because of the effect of anti-symmetrization occasioned by single-nucleon knock-on exchange, making its evaluation difficult; hence, a much simpler approximation, called the zero-range potential, has been used in many nucleus-nucleus calculations [19, 20]. This approach has been used with success in the nucleus-nucleus calculations of heavy-ion optical potential at low energies, but has been found inadequate in refractive scattering, where the data are sensitive to the real optical potential over a wider radial domain. As a consequence, in this work, the study of the HI optical potential for the elastic scattering of the chosen nuclear system at various collision energies of interest is carried out using the finite-range evaluation of the exchange potential by means of the local momentum approximation proposed by Brieva and Rook [21]. This approach has been used with immense success by many researchers previously [7, 9]. Therefore, to solve the non-locality problem, the exact, consistent microscopic approximation of the exchange potential developed by Khoa et al. [7] is employed in this work. Their approach produces an accurate local approximation, resulting from treating the relative motion locally as a plane wave [8].

The exchange potential is computed using an iterative method in this work, ensuring a careful and accurate evaluation of the knock-on exchange effects to obtain a realistic energy dependence of the real folded potential $V(E, R)$, shown from previous calculations [1, 7] to have a much stronger dependence on the exchange term than the intrinsic energy dependence $g(E)$ in Eq. (2). Thus, the volume integral of the real folded potential per interacting nucleon pair, which gives a useful insight into the energy dependence of the real optical potential, is expressed as [7]:

$$J_R(E) = \frac{4\pi N_R}{A_1 A_2} \int_0^\infty [V_D(E, r) + V_{EX}(E, r)] r^2 dr, \quad (6)$$

where A_1 and A_2 represent the two colliding nuclei. In our case, in which a conscious effort is made to assess the performance of the real folded potential derived from the B3Y-Fetal in relation to the M3Y-Reid-based folded potential, this is a very important distinguishing parameter.

Now, considering the fact that the B3Y-Fetal and the M3Y-Reid effective interactions are real, the potential resulting from the double folding model is real and

constitutes the real part of the optical potential in the OM analyses. This real potential, accounting for elastic scattering, is supplemented by an imaginary phenomenological potential that accounts for absorption into non-elastic channels. Therefore, as it is usually practised in this hybrid approach, the imaginary phenomenological part has parameters that are adjusted to give the best fit to the elastic scattering data. Here, we chose the Woods-Saxon shape as the imaginary potential, so that the optical potential in the OM calculations is [7]:

$$\begin{aligned} U(E, R) = & N_R [V_D(E, R) + V_{EX}(E, R)] \\ & - iW_V \left[1 + \exp \left(\left(\frac{R - R_V}{a_V} \right) \right) \right]^{-1} \\ & + 4iW_D a_D \frac{d}{dR} \left[1 + \exp \left(\left(\frac{R - R_D}{a_D} \right) \right) \right]^{-1}, \end{aligned} \quad (7)$$

where W_V and W_D , a_V and a_D , and R_V and R_D are the respective strengths, diffuseness, and radii of the volume (WSV) and surface (WSD) terms of the Woods-Saxon function, respectively [7]. These parameters, alongside the normalization factor N_R , were adjusted to obtain the best fits to the elastic scattering angular distributions. The surface term of Eq. (7) was added for possible improvement of the agreement with the data [7] at certain incident angles. All nuclear densities in the folding model were taken as a two-parameter Fermi distribution with parameters that can reproduce the Shell-Model densities for the nuclei under consideration. All computational analyses of the optical model were carried out using the ECIS-97 code. These OM analyses are used to study the elastic scattering of $^{16}\text{O}+^{16}\text{O}$ at incident energies of 145, 250, 350, and 480 MeV.

4 Results and discussion

Generally, the results obtained with the heavy-ion nucleus-nucleus optical potential used for the study of the elastic scattering of the nuclear system chosen in the present study demonstrate good agreement with results of previous works [7, 8]. The results are presented in both tabular and graphical forms herein and discussed accordingly. For economy of space, we have combined some graphs that have similar features into one figure, and salient points relating to them are appropriately discussed. In discussing the results, attention is given primarily to the results obtained with the optical potential derived from the B3Y-Fetal effective interaction because it is the principal interaction used for folding analyses in this work. The performance of the optical potential based on the M3Y-Reid effective interaction is discussed only when it

becomes necessary to compare it with that of the B3Y-Fetal effective interaction.

The different versions of the M3Y-Reid and B3Y-Fetal interactions in Tables 2 and 3 are based on different versions of DDM3Yn and BDM3Yn density dependences and are grouped together in different groups for the purpose of comparison. Therefore, the DDM3Y1-Reid and DDB3Y1-Fetal interactions are derived from the DDM3Y1 density-dependent version; BDM3Y1-Reid and BDB3Y1-Fetal interactions are from the BDM3Y1 density dependence, BDM3Y2-Reid and BDB3Y2-Fetal are based on the BDM3Y2 density dependence, and BDM3Y3-Reid and BDB3Y3-Fetal interactions are based on the BDM3Y3 density dependence. These density dependences form the basis for comparison of the B3Y-Fetal with the M3Y-Reid effective interaction in the nuclear reaction considered in this study.

4.1 Total real folded potential

The optical model analyses performed in this work have proven beyond reasonable doubt that nuclear matter calculations [11] alone do not suffice for an explicit description of the form and character of the B3Y-Fetal effective interaction. Therefore, the optical potential results shown in Tables 2 and 3, as well as Figs. 1, 2, 3, 4, 5, 6 and 7, are more revealing.

The foremost revelation emanating from the folding analyses is that of form. Figures 1 and 2 unambiguously show that one of the underlying reasons for the performance difference is closely associated with the fact that different effective interactions have different forms. Figure 1 reveals that the optical potential based on the B3Y-Fetal interaction has a repulsive direct term (Eq.(5)), which is combined with an attractive exchange term (Eq. (5)) of large magnitude to produce a total real folded potential that is attractive. In contrast, Fig. 2 shows that the optical potential involving the M3Y-Reid interaction has an attractive direct term and an attractive exchange term of approximately the same magnitude that combine to form an attractive total real folded potential. This basic difference between the two interactions was observed during folding analyses to have been translated into the response of each effective interaction to the elastic scattering data in various ways.

Figure 1 shows the repulsive direct $V_D(E,R)$ and attractive exchange $V_{EX}(E,R)$ contributions to the total real folded potential for the $^{16}\text{O}+^{16}\text{O}$ system, computed with the DDB3Y1-Fetal interaction at incident energies from 9 to 30 MeV/nucleon. The plots clearly show that most of the energy dependence of the HI optical potential

comes from the exchange term, which dominates at smaller inter-nuclear distances, especially at low energies; this suggests that the density-dependent contribution from V_{EX} is also much stronger than that from V_D . However, the contribution of V_{EX} becomes comparable to and even less than that of V_D as the overlap density decreases exponentially in the surface region. Thus, the total HI potential is dominated by the direct component at distances $R \geq 7$ fm, and this explains why the simple folding model [1] has been very successful in cases where the scattering data is only sensitive to the tail of the optical potential.

It is also evident from Fig. 1 that the exchange potential becomes less dominant with increasing incident energy, so that both the exchange and direct potentials have approximately the same strength even at small distances. The result is that the total real HI potential becomes increasingly repulsive with incident energy; this is in good agreement with the work of [7].

θ_r , the fact that the absolute strength of the total real folded potential is governed to some extent by the shape of the chosen effective NN forces makes it quite clear that the real folded potentials based on the B3Y-Fetal become more repulsive at higher incident energies than their counterparts based on M3Y-Reid, whose direct and exchange components are attractive, as shown in Fig. 2. Therefore, when compared with the total HI potential of DDM3Y1-Reid, the total HI potential of DDB3Y1-Fetal becomes more repulsive with increasing bombarding energy because of its peculiar nature.

4.2 Fits to $^{16}\text{O}+^{16}\text{O}$ elastic data

The elastic scattering of this system was studied at incident energies of 145, 250, 350, and 480 MeV. All experimental data were obtained from Khoa et al. [7, 8] through helpful communication. The data at $E_{\text{Lab}} = 250, 350, \text{ and } 480$ MeV were originally measured using the Q3D magnetic spectrometer at the cyclotron of the Hahn-Meitner Institute (HMI) in Berlin, Germany [22–24], while the data at $E_{\text{Lab}} = 145$ MeV were measured by Sugiyama et al. at the Japan Atomic Energy Research Institute (JAERI) in Tokai [25]; all these data were obtained by Khoa et al. [7, 8] through collaboration.

The results produced by various real folded potentials with the volume WS imaginary potential are presented in Table 2 and plotted in Fig. 3. In each case, a reasonable agreement with the experimental data throughout the entire angular range can be observed. The deep DDB3Y1-Fetal and BDB3Y1-Fetal folded potentials proved to be the best, reproducing the data over the entire angular range. The BDB3Y3-Fetal potential, followed by the BDB3Y2-Fetal potential, had the poorest performance, providing an

Table 2 Optical parameters used in the folding analyses of the elastic $^{16}\text{O}+^{16}\text{O}$ scattering data at $E_{\text{lab}} = 145\text{--}480$ MeV. The results obtained in Ref. [7] with the M3Y-Reid interaction are in brackets

Potential	N_{R}	$-J_{\text{R}}$ (MeVfm ³)	$\langle r_{\text{R}}^2 \rangle^{\frac{1}{2}}$ (fm)	W_{V} (MeV)	R_{V} (fm)	a_{V} (fm)	σ_{R} (mb)	χ^2
[$^{16}\text{O}+^{16}\text{O}$, $E_{\text{Lab}} = 145$ MeV]								
DDM3Y1-REID	0.8526 (0.9445)	336.3 (339.0)	4.2130 (4.1574)	17.533 (17.133)	6.0028 (6.0028)	0.6905 (0.6905)	1703 (1693)	26.2 (53.4)
DDB3Y1-FETAL	0.8548	332.1	4.1813	17.638	6.0028	0.6905	1700	18.3
BDM3Y1-REID	0.8782 (0.9653)	340.5 (340.3)	4.2135 (4.1597)	18.767 (17.490)	5.9726 (5.9726)	0.7001 (0.7011)	1725 (1702)	20.4 (55.4)
BDB3Y1-FETAL	0.8688	332.1	4.1812	17.929	5.9726	0.7001	1706	19.0
BDM3Y2-REID	0.9210 (1.0154)	344.2 (344.4)	4.2205 (4.1706)	19.829 (18.531)	5.9176 (5.9176)	0.7128 (0.7128)	1737 (1714)	22.4 (59.8)
BDB3Y2-FETAL	0.9108	336.4	4.1867	18.823	5.9176	0.7128	1716	20.5
BDM3Y3-REID	0.9345 (1.0588)	352.1 (341.2)	4.2286 (4.2075)	22.926 (22.601)	5.8798 (5.8798)	0.6552 (0.6552)	1679 (1673)	27.4 (70.9)
BDB3Y3-FETAL	0.9605	309.7	4.3863	22.335	5.8798	0.6552	1669	29.1
[$^{16}\text{O}+^{16}\text{O}$, $E_{\text{Lab}}=250$ MeV]								
DDM3Y1-REID	0.7637 (0.8905)	283.1 (303.7)	4.2134 (4.1650)	29.427 (28.498)	5.6184 (5.6184)	0.7368 (0.7368)	1772 (1762)	14.6 (46.0)
DDB3Y1-FETAL	0.8209	298.6	4.1817	29.281	5.6184	0.7368	1771	10.1
BDM3Y1-REID	0.7835 (0.9099)	285.4 (304.7)	4.2142 (4.1675)	29.188 (28.429)	5.6418 (5.6318)	0.7349 (0.7349)	1777 (1763)	15.6 (48.4)
BDB3Y1-FETAL	0.8366	299.4	4.1819	28.933	5.6418	0.7349	1774	10.4
BDM3Y2-REID	0.8135 (0.9510)	285.7 (306.3)	4.2219 (4.1788)	29.177 (28.360)	5.6600 (5.6600)	0.7299 (0.7299)	1783 (1767)	17.5 (57.0)
BDB3Y2-FETAL	0.8727	301.7	4.1879	28.745	5.6600	0.7339	1778	11.8
BDM3Y3-REID	0.8233 (0.9866)	291.9 (301.8)	4.2293 (4.2160)	29.238 (28.270)	5.7002 (5.7002)	0.7131 (0.7002)	1767 (1762)	18.0 (74.6)
BDB3Y3-FETAL	0.8270	247.8	4.3999	28.459	5.7002	0.7131	1755	16.6
[$^{16}\text{O}+^{16}\text{O}$, $E_{\text{Lab}}=350$ MeV]								
DDM3Y1-REID	0.8450 (0.9218)	295.4 (299.4)	4.2149 (4.1728)	33.274 (31.628)	5.6099 (5.6099)	0.6534 (0.6534)	1660 (1642)	9.0 (40.2)
DDB3Y1-FETAL	0.8566	292.7	4.1833	32.669	5.6099	0.6534	1652	7.9
BDM3Y1-REID	0.8724 (0.9435)	299.6 (300.9)	4.2160 (4.1754)	32.176 (31.430)	5.6766 (5.6366)	0.6470 (0.6470)	1669 (1642)	7.9 (41.2)
BDB3Y1-FETAL	0.8735	293.6	4.1837	31.516	5.6766	0.6470	1659	7.9
BDM3Y2-REID	0.9150 (0.9942)	302.6 (304.8)	4.2242 (4.1870)	32.5583 (30.980)	5.7042 (5.6999)	0.6330 (0.6330)	1663 (1645)	8.8 (43.4)
BDB3Y2-FETAL	0.9164	297.4	4.1903	31.585	5.7042	0.6330	1651	8.0
BDM3Y3-REID	0.9141 (1.0369)	306.1 (301.7)	4.2309 (4.2248)	33.458 (31.914)	5.7148 (5.7048)	0.6301 (0.6301)	1671 (1652)	9.4 (48.6)
BDB3Y3-FETAL	1.0556	294.8	4.4149	36.870	5.7148	0.6301	1701	14.6
[$^{16}\text{O}+^{16}\text{O}$, $E_{\text{Lab}}=480$ MeV]								
DDM3Y1-REID	0.8018 (0.8520)	259.9 (259.8)	4.2184 (4.1838)	33.505 (32.675)	5.3784 (5.3984)	0.7434 (0.7434)	1662 (1657)	8.7 (6.7)
DDB3Y1-FETAL	0.7987	251.6	4.1871	32.790	5.3784	0.7434	1652	8.5
BDM3Y1-REID	0.8119 (0.8741)	258.5 (261.6)	4.2198 (4.1866)	32.531 (32.517)	5.42774 (5.4274)	0.7377 (0.7377)	1664 (1660)	8.9 (6.9)

Table 2 continued

Potential	N_R	$-J_R$ (MeVfm ³)	$\langle r_R^2 \rangle^{\frac{1}{2}}$ (fm)	W_V (MeV)	R_V (fm)	a_V (fm)	σ_R (mb)	χ^2
BDB3Y1-FETAL	0.8044	249.2	4.1878	31.715	5.4274	0.7377	1653	9.2
BDM3Y2-REID	0.9765 (0.9116)	299.3 (262.2)	4.2288 (4.1986)	33.183 (32.988)	5.7948 (5.6948)	0.6030 (0.6030)	1638 (1588)	19.8 (10.5)
BDB3Y2-FETAL	0.9783	292.5	4.1950	33.999	5.7008	0.6030	1602	13.0
BDM3Y3-REID	0.8272 (1.0224)	257.4 (278.9)	4.2342 (4.2370)	33.700 (33.521)	5.4213 (5.5213)	0.7503 (0.7503)	1692 (1735)	11.0 (10.6)
BDB3Y3-FETAL	0.9445	240.6	4.4370	35.121	5.4213	0.7503	1709	11.0

Table 3 Optical parameters for the folding analyses of ¹⁶O+¹⁶O elastic scattering data at $E_{lab} = 250$ and 350 MeV with imaginary Pot. = WSV + WSD

Potential	N_R	W_V (MeV)	R_V (fm)	a_V (fm)	W_D (MeV)	R_D (fm)	a_D (fm)	σ_R (mb)	χ^2
[¹⁶ O+ ¹⁶ O, $E_{Lab}=250$ MeV (WSV+WSD)]									
DDM3Y1-REID	0.7764 (0.8905)	37.433 (36.641)	4.7915 (4.7915)	0.9062 (0.9062)	3.5230 (3.5230)	5.8309 (5.8309)	0.4268 (0.4268)	1830 (1822)	11.2 (37.4)
DDB3Y1-FETAL	0.8336	38.086	4.7915	0.9062	3.5230	5.8309	0.4268	1836	9.8
BDM3Y1-REID	0.7945 (0.9099)	38.620 (37.876)	4.7039 (4.7083)	0.9212 (0.9219)	3.9878 (3.9878)	5.8064 (5.8064)	0.4267 (0.4267)	1835 (1829)	10.7 (37.2)
BDB3Y1-FETAL	0.8499	39.2118	4.7038	0.9212	3.9878	5.8064	0.4267	1841	9.4
BDM3Y2-REID	0.8259 (0.9510)	38.056 (38.528)	4.6464 (4.6464)	0.9313 (0.9313)	5.1053 (5.1053)	5.7267 (5.7267)	0.4231 (0.4231)	1827 (1831)	10.0 (37.6)
BDB3Y2-FETAL	0.8830	38.804	4.6464	0.9313	5.1013	5.7267	0.4231	1833	9.0
BDM3Y3-REID	0.8269 (0.9866)	39.258 (39.836)	4.6109 (4.6109)	0.9355 (0.9355)	5.6530 (5.6530)	5.7518 (5.7518)	0.4012 (0.4012)	1830 (1835)	9.5 (37.6)
BDB3Y3-FETAL	0.8836	39.745	4.6109	0.9355	5.6530	5.7518	0.4012	1834	10.8
[¹⁶ O+ ¹⁶ O, $E_{Lab}=350$ MeV (WSV+WSD)]									
DDM3Y1-REID	0.8416 (0.9218)	29.9001 (25.265)	5.7554 (5.7554)	0.6488 (0.6488)	7.9655 (7.9655)	4.7371 (4.7371)	0.3637 (0.3637)	1683 (1634)	8.1 (39.8)
DDB3Y1-FETAL	0.8452	29.676	5.7554	0.6488	7.9655	4.7371	0.3637	1678	10.9
BDM3Y1-REID	0.8560 (0.9435)	30.079 (25.429)	5.7578 (5.7578)	0.6481 (0.6481)	7.4643 (7.4643)	4.7473 (4.7473)	0.3823 (0.3823)	1685 (1637)	8.2 (40.6)
BDB3Y1-FETAL	0.8624	29.814	5.7578	0.6481	7.4643	4.7473	0.3823	1679	10.8
BDM3Y2-REID	0.9057 (0.9942)	30.704 (25.929)	5.7612 (5.7612)	0.6458 (0.6458)	6.2634 (6.2634)	4.8143 (4.8143)	0.4240 (0.4240)	1690 (1645)	8.4 (42.3)
BDB3Y2-FETAL	0.9037	30.226	5.7612	0.6458	6.2634	4.8143	0.4240	1682	10.3
BDM3Y3-REID	0.9050 (1.0369)	31.690 (26.304)	5.7692 (5.7692)	0.6309 (0.6309)	4.5614 (4.5614)	4.9566 (4.9566)	0.5031 (0.5031)	1680 (1644)	8.8 (51.5)
BD3Y3-FETAL	0.8363	28.753	5.6792	0.6309	4.5614	4.9566	0.5031	1646	18.4

The results obtained in Ref. [7] using the M3Y-Reid interaction are in brackets

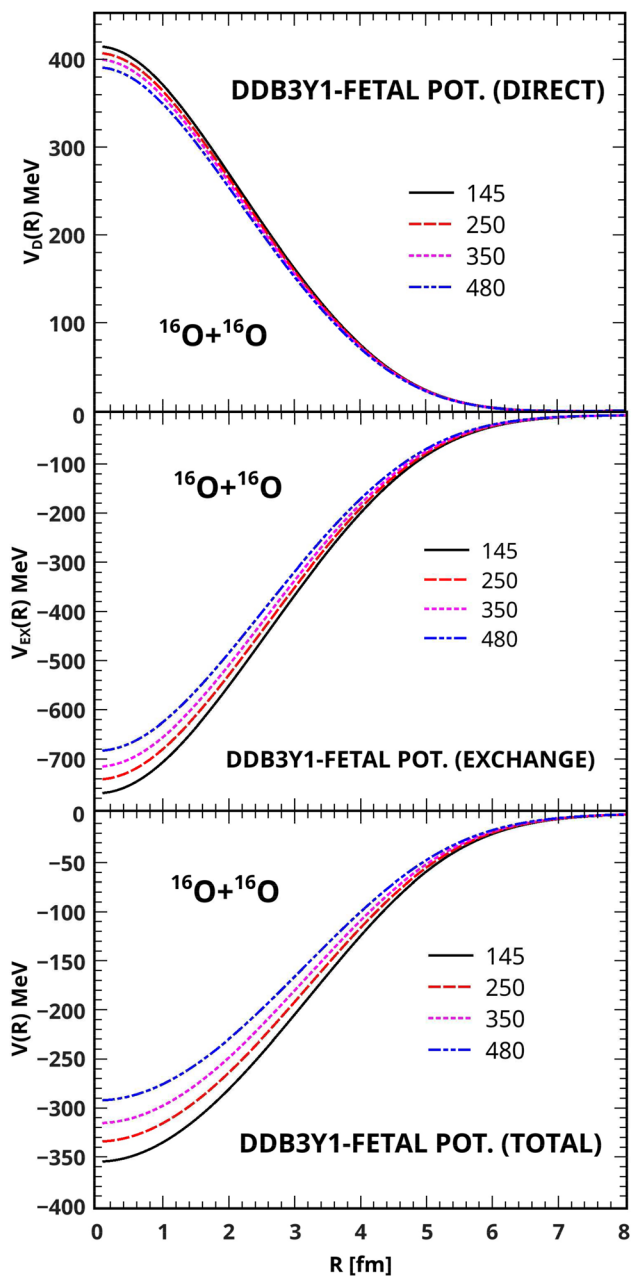


Fig. 1 (Color online) Direct (upper part) and exchange (middle) contributions to the total folded DDB3Y1-Fetal potential (lower part) for the $^{16}\text{O} + ^{16}\text{O}$ system at incident energies of 145, 250, 350, and 480 MeV

incorrect description of the data at large angles. On average, the renormalization of the real folded potentials in these cases is approximately 0.85, giving J_R values of the real optical potential that are very close to those obtained by Khoa and co-researchers [7].

To improve the agreement of the calculated cross sections with the data in the large-angle (refractive) region at 250 and 350 MeV, a surface WS term, WSD, was added to the imaginary potential, with the real folded potentials kept

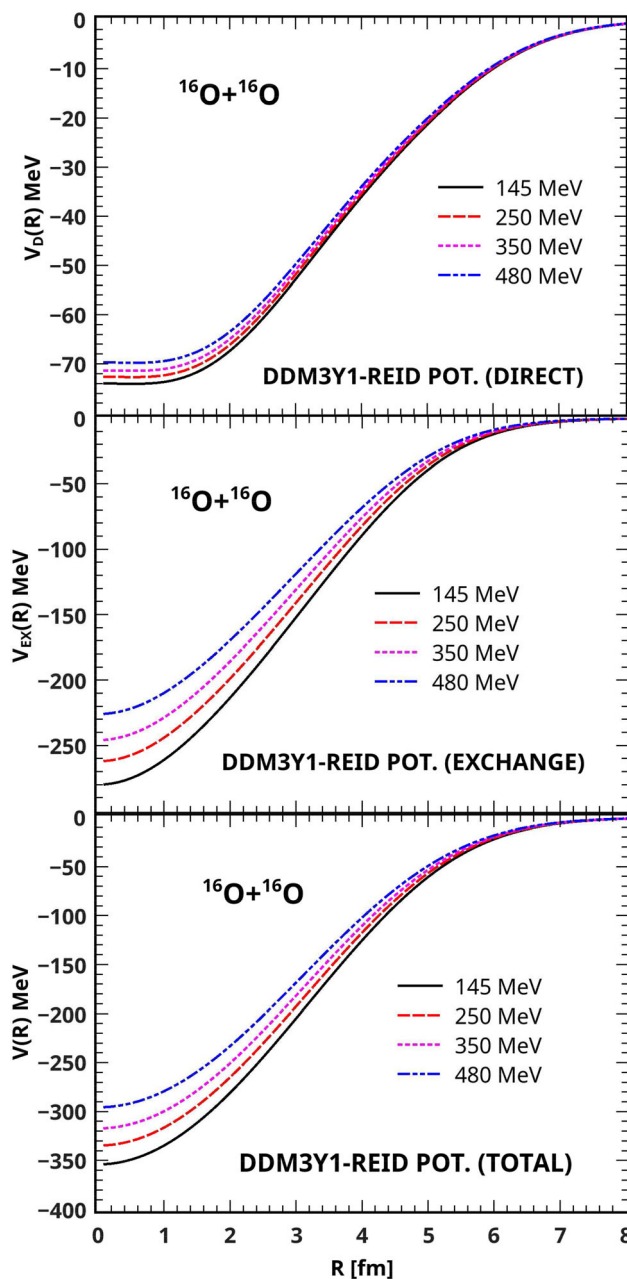


Fig. 2 (Color online) Direct (upper part) and exchange (middle) contributions to the total folded DDM3Y1-Reid potential (lower part) for the $^{16}\text{O} + ^{16}\text{O}$ system at incident energies of 145, 250, 350, and 480 MeV

fixed to determine the effects of the imaginary potential. Consequently, the surface WSD potential did improve fits to the data at 250 and 350 MeV, respectively. The improved fits are, respectively, recorded in Table 3 and plotted in Figs. 4 and 5. As recorded in Tables 3a and 3b, the improved fits are more pronounced at 250 MeV than at 350 MeV. Clearly, a comparison of Tables 3a and 3b, representing $E_{\text{Lab}} = 250$ MeV, shows that the values of χ^2 in Table 3a are generally lower; this indicates improved fits.

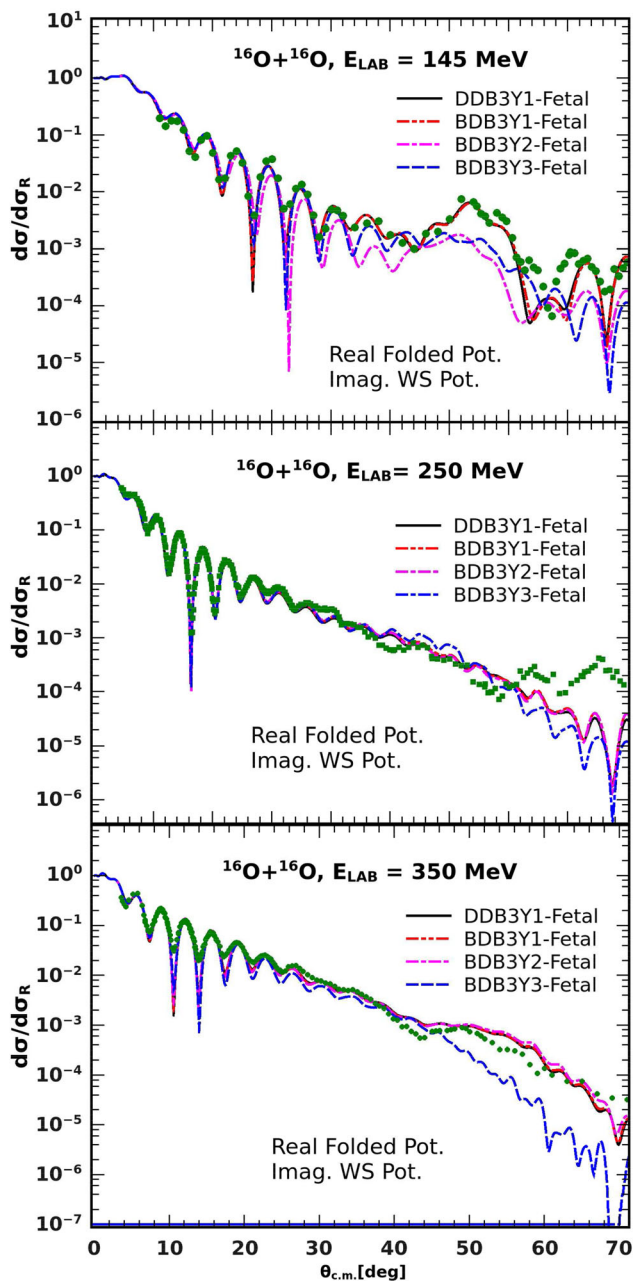


Fig. 3 (Color online) Fits to $^{16}\text{O} + ^{16}\text{O}$ Elastic Data at $E_{\text{Lab}} = 145, 250, \text{ and } 350$ MeV (in Table 1) obtained with different B3Y-Fetal-based folded potentials and volume Woods–Saxon optical potentials (experimental data were originally measured in Refs. [24, 25])

Quantitatively, the values of χ^2 in Table 3a obtained in this work with the DDM3Y1-Reid, BDM3Y1-Reid, BDM3Y2-Reid, and BDM3Y3-Reid are 9.0, 7.9, 8.8 and 9.4 (with WSD) versus 14.6, 15.6, 17.5, and 18.0, respectively, in Table 1b (without WSD). Comparing these two sets of values of χ^2 , the differences (reductions) in the values of χ^2 obtained with the DDM3Y1-Reid, BDM3Y1-Reid, BDM3Y2-Reid, and BDM3Y3-Reid potentials with the inclusion of WSD are 5.6, 7.7, 8.7, and 8.6, respectively;

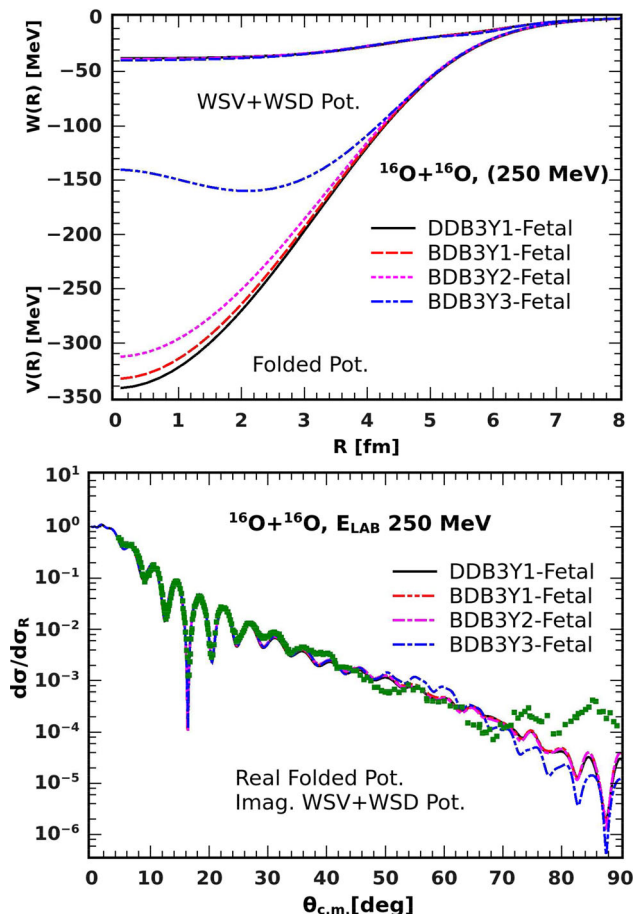


Fig. 4 (Color online) Fits to $^{16}\text{O} + ^{16}\text{O}$ elastic data at $E_{\text{Lab}} = 250$ MeV (lower part) with the radial shapes of the real folded $V(R)$ and the Woods–Saxon [$W(R)=WSV+WSD$] imaginary potentials (upper part) used in OM analyses. The experimental data were originally measured in Ref. [24])

these represent improved fits. Similarly, the B3Y-Fetal-based potentials DDB3Y1-Fetal, BDB3Y1-Fetal, BDB3Y2-Fetal, and BDB3Y3-Fetal are shown in Table 3a to produce 9.8, 9.4, 9.0, and 10.8, respectively, as values of χ^2 at 250 MeV (with WSD). When these values are compared with 10.1, 10.4, 11.8, and 16.6, obtained with the same set of folded potentials (arranged in the same order) as the values of χ^2 in Table 2b (without WSD), the differences (reductions) in the values of χ^2 with the inclusion of WSD are 0.3, 1.0, 2.8, and 5.8, respectively, indicating some improvement of the fits at 250 MeV. Here, without WSD, the fits are worse for the M3Y-Reid than for the B3Y-Fetal-based potentials in Table 2b; therefore, with the inclusion of WSD in Table 3a, the improvement of the fits is more pronounced for the former than for the latter. The fact is that the inclusion of WSD in our optical model analysis has actually improved the fits, but the improvement cannot be clearly seen with the eye in Figs. 4 and 5. This is in agreement with the results of Ref. [7], which suggest that a

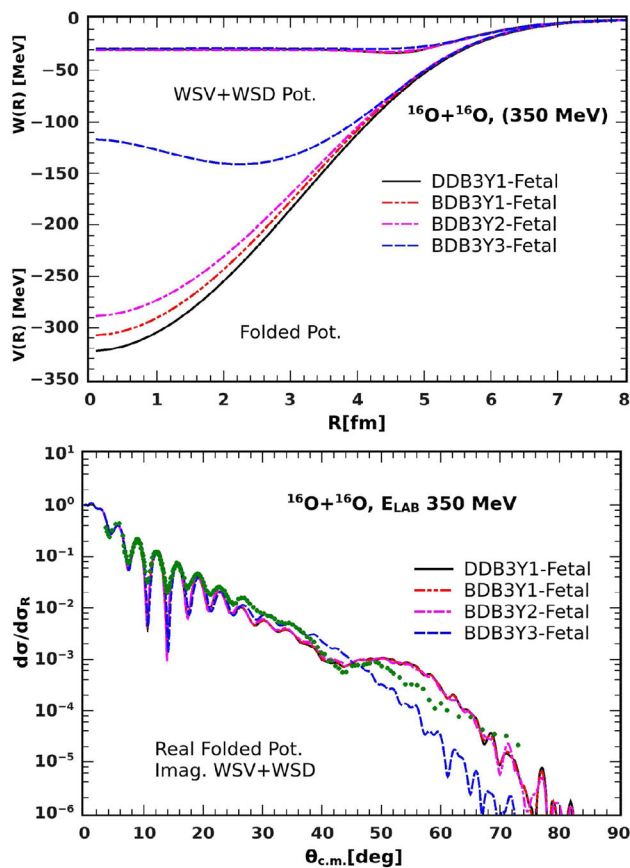


Fig. 5 (Color online) Fits to $^{16}\text{O} + ^{16}\text{O}$ elastic data at $E_{\text{Lab}} = 350$ MeV (lower part) based on B3Y-Fetal with radial shapes of real folded $V(R)$ and Woods–Saxon [$W(R)=WSV+WSD$] imaginary potentials (upper part). The experimental data were originally measured in Refs. [23, 24]

combination of the imaginary potentials makes the absorption at the surface strong enough to reproduce the diffractive part of the scattering, while the absorption at small distances becomes weaker (upper part of Fig. 5), giving rise to a broad maximum in the elastic cross section. (the lower part of Fig. 5). With the M3Y-Reid-based potentials, the improvement of fits at 350 MeV is marginal. In Table 3b, the DDM3Y1-Reid, BDM3Y1-Reid, BDM3Y2-Reid, and BDM3Y3-Reid produced 8.1, 8.2, 8.4, and 8.8, respectively, as values of χ^2 at 350 MeV (with WSD added), compared with 9.0, 7.9, 8.8, and 9.4, respectively, in Table 2c (without WSD), and the corresponding differences (reductions) are 0.8, 0.3, 0.4, and 0.6, respectively. In this case, a difference of only 0.3 does not indicate an improved fit, whereas the others are marginal differences that represent improved fits. When the differences obtained with these potentials at 250 MeV are compared with the differences observed at 350 MeV, it is evident that the improved fits were more pronounced at 250 MeV than at 350 MeV. Figure 6 shows the improved fit obtained with the M3Y-Reid at 350 MeV to show that the

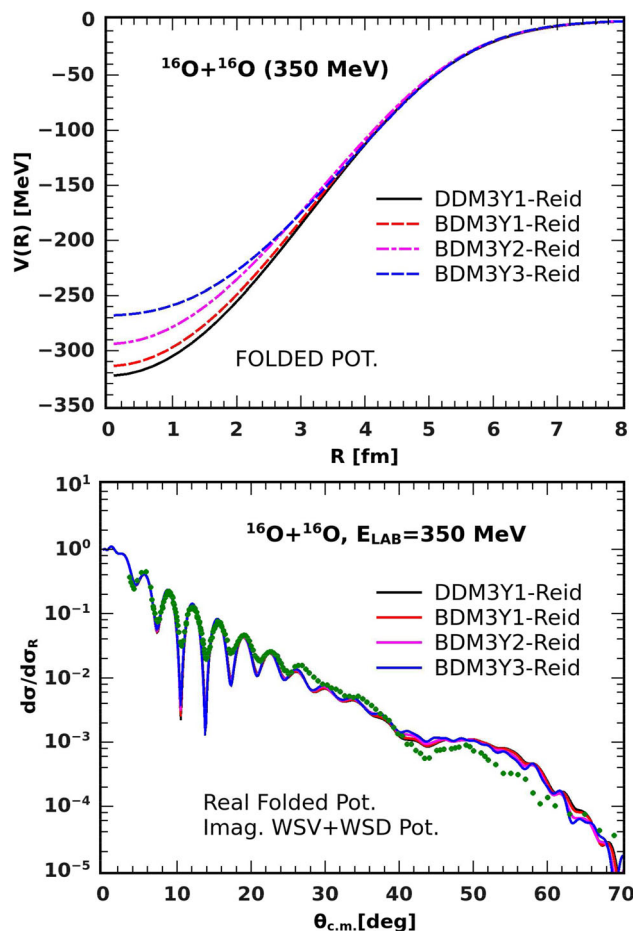


Fig. 6 (Color online) Fits to $^{16}\text{O} + ^{16}\text{O}$ elastic data at $E_{\text{Lab}} = 350$ MeV involving Woods–Saxon [$W(R)=WSV+WSD$] imaginary potential (lower part) based on M3Y-Reid with radial shapes of the real folded $V(R)$ potential (upper). The experimental data were originally measured in Refs. [22, 24]

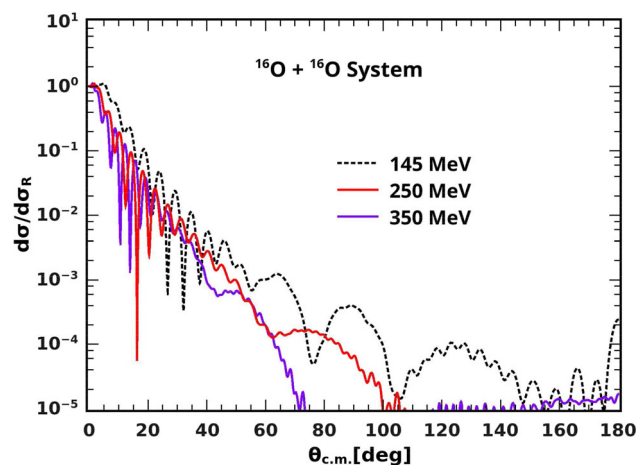


Fig. 7 (Color online) Unsymmetrized OM calculations of the $^{16}\text{O} + ^{16}\text{O}$ system at $E_{\text{LAB}} = 145, 250,$ and 350 MeV using the best-fit DDB3Y1-Fetal folded potential

folded potentials derived from the B3Y-Fetal are in good agreement by comparison. Even though the fits have been improved at these energies, the relative differences in the shapes of the different folded potentials remain practically the same, but it is noteworthy that the best fit to the large-angle data is given by the DDM3Y1 and BDM3Y1 versions of the folded potentials, which are the most realistic folded potentials.

From the past work [5, 7], several OM analyses of the data at 350 MeV have revealed that the broad maximum near 50° , identified as a remnant of the primary rainbow, (with the first Airy minimum around 44°), can only be reproduced by real optical potentials that are deep enough to belong to the group of refractive potentials. Accordingly, the results of the present work have shown the best-fit folded potentials that consistently produce the evolution of Airy oscillation with energy to be deeply refractive.

To show and confirm this, we have followed the procedure of Khoa and collaborators [7] to plot the elastic scattering cross sections arising from the unsymmetrized calculations of the $^{16}\text{O}+^{16}\text{O}$ system at 145, 250, and 350 MeV obtained with the best-fit folded potential, DDB3Y1-Fetal, in Fig. 7 for the sole purpose of studying the evolution of the rainbow pattern, in which Airy minima were observed to shift smoothly toward small scattering angles with increasing incident energy. The plots show the existence of Airy minima at the aforementioned energies. Thus, at an energy of 145 MeV, the first Airy minimum occurs at 100° , followed by the second at 75° and the third at 48° . What is interesting here is the continuous shifting of the Airy minima toward the diffractive region as the incident energy increases. Accordingly, it can be seen from Figure 10 that the first Airy minimum shifts from approximately 100° at the energy of 145 MeV to approximately 66° at 250 MeV (solid curve), and at 350 MeV, it is seen to have shifted to approximately 44° . This shows that our version of the folding model, derived from the B3Y-Fetal, has proven to be a reliable HI optical potential at different energies with the DDB3Y1- or BDB3Y1-Fetal potential as a trustworthy tool to predict scattering cross sections at large angles.

4.3 Energy dependence of the real HI potential

Many folding analysis results have shown that the renormalization factor N_R of the real folded potential should be very close to unity for the model used for the nucleus–nucleus potential to be adjudged satisfactorily realistic [7, 8]. However, higher-order terms such as dynamic polarization correction, which is mostly repulsive and surface-peaked, contribute to both the real and imaginary parts of the HI potential, where the folded potential is

a first-order term. N_R smaller than one might be considered reasonable [7]. Consequently, the N_R values ranging from 0.8 to 0.9 obtained in the present folding analyses can be considered reasonable.

Furthermore, all N_R values obtained using the best-fit real folded potential (DDB3Y1-Fetal and DDM3Y1-Reid) in the analyses of ^{16}O and ^{12}C scattering data are plotted against the incident energy in the upper regions of Figs. 8 and 9. The plots show that N_R depends weakly on energy and varies around a value of 0.9. The BDM3Y1 exhibits the same behavior.

Therefore, it is evident that the intrinsic energy dependence arising from the exchange effects and the weak explicit energy dependence $g(E)$ factor introduced into the effective NN interaction in Eq. (6) are actually the main sources of the total energy dependence of the real HI optical potential.

In the lower regions of Figs. 8 and 9, the volume integral of the real folded potential per interacting nucleon pair J_R is seen to decrease smoothly from approximately 340–150 MeV fm³ as the incident energy increases from approximately 10–120 MeV/nucleon. This trend agrees well with previous studies. [7], which shows that prediction

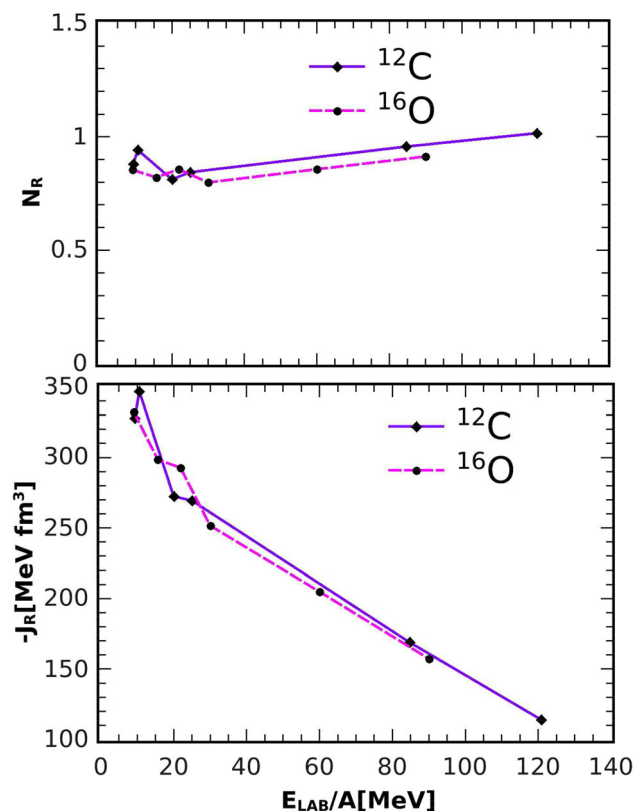


Fig. 8 (Color online) Energy dependence of the renormalization factor N_R (upper part) and volume integral J_R (lower part) of the DDB3Y1-Fetal potential deduced from the folding analyses of the elastic ^{16}O and ^{12}C scattering data at energies up to 120 MeV/nucleon

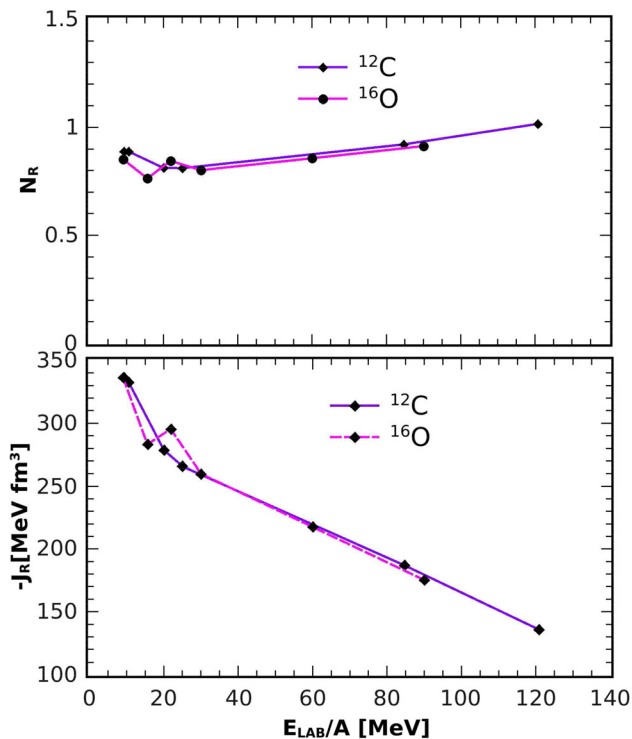


Fig. 9 (Color online) Energy dependence of the renormalization factor N_R (upper part) and volume integral J_R (lower part) of the DDM3Y1-Reid potential deduced from the folding analyses of the elastic ^{16}O and ^{12}C scattering data at energies up to 120 MeV/nucleon

of the energy dependence of the real HI potential using the folding model in this work is reliably satisfactory.

Regarding the overall performance of the two effective interactions in the OM analyses of elastic scattering data, it is worth noting that the B3Y-Fetal has so far demonstrated acceptable agreement with the M3Y-Reid. Tables 2 and 3 show that the values of the renormalization factor N_R obtained with the B3Y-Fetal are slightly higher than those obtained with the M3Y-Reid, so that the corresponding reaction cross sections σ_R for the former are lower than those for the latter in almost all cases. This level of performance by B3Y-Fetal is quite impressive. A well-established trend that both interactions portray is one in which the optical potential becomes progressively repulsive as the incident energy increases, which is in agreement with the work of Nuclear Physics scholars [1, 7].

4.4 EOS of normal nuclear matter

The folding analyses in this study have shown that the DDM3Y1-Fetal ($K = 176$ MeV) and BDM3Y1-Fetal ($K = 235$ MeV) are the best-fit and most realistic optical potentials. This is also true for the folded potentials derived from M3Y-Reid (DDM3Y1- and BDM3Y1-Reid) effective interactions. When these results bear on the results of

nuclear matter calculations reproduced and discussed in Sect. 2 (page 6), a strong factual link for establishing the nature of the EOS of symmetric nuclear matter (SNM) using incompressibility values clearly evolves. It is known that the incompressibilities of 351 MeV and 467 MeV produced by the BDB3Y2-Fetal and BDB3Y3-Fetal represent stiff EOS of SNMs [3, 12]. These interactions are shown in Figs. 1 and 2 to be more repulsive and in Figs. 3, 4, 5 to provide a very bad description of the elastic data of the $^{16}\text{O}+^{16}\text{O}$ system, whereas the DDB3Y1- and BDB3Y1-Fetal, with incompressibilities of 176 MeV and 235 MeV, respectively, are shown to be better and in good agreement. Because the well-known standard is that the theoretical EOSs that predict higher K_0 values of approximately 300 MeV are often called “stiff”, whereas those that predict smaller K_0 values of approximately 200 MeV are said to be “soft” [12], the agreement demonstrated by the DDB3Y1- and BDB3Y1-Fetal herein shows that cold nuclear matter possibly has an underlying soft EOS. An additional important conclusion may be drawn from the present study of refractive HI scattering: the corresponding nuclear incompressibility $K = 170\text{--}240$ MeV [7] is the most realistic EOS for cold nuclear matter. It is hoped that this conclusion will be of great interest for some studies [26, 27] in Astrophysics where the nuclear EOS [28] is a key component of the calculation.

5 Conclusion

The focus of this paper is the study of the elastic scattering of $^{16}\text{O} + ^{16}\text{O}$ nuclei using a heavy-ion nucleus–nucleus optical potential based on four types of real folded potential derived from a new M3Y-type effective interaction called the B3Y-Fetal interaction within the framework of an optical model. The major findings of this study are summarized in the following concluding statements.

- Folding analyses are observed in this work to be a computational necessity for a complete description of the form and character of the B3Y-Fetal interaction. Figure 1 provides convincing information concerning the form and character of this new effective interaction, which was not revealed in nuclear matter calculations in our earlier paper [11].
- The basic difference between the optical potentials derived from the M3Y-Reid and B3Y-Fetal interactions, in terms of form and character, is closely tied to their direct components. The optical potential based on the B3Y-Fetal has a repulsive direct component, whereas the one based on M3Y-Reid has an attractive direct component.

- The heavy-ion optical potential derived from the B3Y-Fetal has been found to be deep and attractive at small inter-nuclear distances, especially at low energies, as shown in Fig. 1. Furthermore, it has demonstrated weak absorption in the chosen nuclear system.
- Results have shown the DDB3Y1-Fetal and BDB3Y1-Fetal to be the best-fit folded potentials, followed by the BDB3Y2-Fetal, with the BDB3Y3-Fetal as the optical potential with the poorest fit to the elastic data of the nuclear system at all energies considered in this work. This trend of performance of the optical potentials, which is also true for the optical potentials based on the M3Y-Reid interaction, is again in excellent agreement with the findings of Khoa et al. [7].
- The best-fit folded potentials, DDB3Y1- and BDB3Y1-Fetal, were found to reproduce reasonably well the energy dependence of the real optical potential for ^{16}O scattering found in previous OM analyses. The results obtained herein also show them to be of the family of deep refractive potentials, as they consistently describe Airy-like structures at large scattering angles observed in the ^{16}O scattering data at different energies. In addition, the folding analyses in this study of this family of folded potentials, known to have microscopically generated a nuclear matter equation of state with incompressibility $K = 176\text{--}235$ MeV [11], suggest strongly that cold nuclear matter is governed by a soft EOS.

On a final note, the performance of the B3Y-Fetal in optical model analyses has been compared with that of the M3Y-Reid interaction, and the agreement between them has been found to be quite impressive, as they were seen to overlap and overtake each other with a marginal performance gap at various points in our OM analyses.

Acknowledgements Prof. Dao T. Khoa of the Institute for Nuclear Science and Technology (INST), Vietnam, is specially and gratefully acknowledged for providing helpful academic materials and excellent guidance in this work.

Author contributions Both authors contributed to the study conception and design. Material preparation, data gathering and analysis were performed by Isaiah Ochala, supervised by Joseph O. Fiase. The first draft of the manuscript was written by Isaiah Ochala, and both authors commented on previous versions of the manuscript. The authors jointly read and approved final manuscript.

References

1. G.R. Satchler, W.G. Love, Folding model potentials from realistic interactions for heavy-ion scattering. *Phys. Rep. (Rev. Sect. Phys. Lett.)* **55**, 183–254 (1979). [https://doi.org/10.1016/0370-1573\(79\)90081-4](https://doi.org/10.1016/0370-1573(79)90081-4)
2. D.T. Khoa, V.W. Oertzen, H.G. Bohlen et al., Study of diffractive and refractive structure in the elastic $^{16}\text{O} + ^{16}\text{O}$ scattering at incident energies ranging from 124 to 1120 MeV. *Nuclear Phys. A* **672**, 387–416 (2000). [https://doi.org/10.1016/S0375-9474\(99\)00856-8](https://doi.org/10.1016/S0375-9474(99)00856-8)
3. M.E. Brandan, G.R. Satchler, The interaction between light heavy ions and what it tells us. *Phys. Rep.* **285**, 143–243 (1997). [https://doi.org/10.1016/S0370-1573\(96\)00048-8](https://doi.org/10.1016/S0370-1573(96)00048-8)
4. D.T. Khoa, E. Khan, G. Colo et al., Folding model analysis of elastic and inelastic proton scattering on sulphur isotopes. *Nuclear Phys. A* **706**, 61–84 (2002). [https://doi.org/10.1016/S0375-9474\(02\)00866-7](https://doi.org/10.1016/S0375-9474(02)00866-7)
5. M. Katsuma, Y. Sakuragi, S. Okabe et al., Coupled-channels study of the nuclear rainbow phenomenon for the $^{12}\text{C} + ^{16}\text{O}$ system. *Prog. Theor. Phys.* **107**, 377 (2002). <https://doi.org/10.1143/PTP.107.377>
6. S.M. Wong, *Introductory Nuclear Physics*, 2nd edn. (Prentice-Hall International Inc, Toronto, 2004). <https://doi.org/10.1002/9783527617906>
7. D.T. Khoa, V.W. Oertzen, H.G. Bohlen, Double-folding model for heavy-ion optical potential: revised and applied to study ^{12}C and ^{16}O elastic scattering. *Phys. Rev. C* **49**, 1652 (1994). <https://doi.org/10.1103/PhysRevC.49.1652>
8. D.T. Khoa, G.R. Satchler, W.V. Oertzen, Nuclear incompressibility and density dependent NN interactions in the folding model for nucleus potentials. *Phys. Rev. C* **56**, 954 (1997). <https://doi.org/10.1103/PhysRevC.56>
9. G.R. Satchler, *Introduction to Nuclear Reactions*, 2nd edn. (Macmillan Education Ltd, London, 1990). <https://doi.org/10.1007/978-1-349-20532-8>
10. J.O. Fiase, K.R.S. Devan, A. Hosaka, Mass dependence of M3Y-type interactions and the effects of tensor correlations. *Phys. Rev. C* **66**, 014004 (2002). <https://doi.org/10.1103/PhysRevC.66.014004>
11. I. Ochala, J.O. Fiase, Symmetric nuclear matter calculations—a variational approach. *Phys. Rev. C* **98**, 064001 (2018). <https://doi.org/10.1103/PhysRevC.98.064001>
12. D.T. Khoa, V.W. Oertzen, Refractive alpha-nucleus scattering; a probe for the incompressibility of cold nuclear matter. *Phys. Lett. B* **342**, 6–12 (1995). [https://doi.org/10.1016/0370-2693\(94\)01393-Q](https://doi.org/10.1016/0370-2693(94)01393-Q)
13. P.E. Hodgson, *The Nucleon Optical Model* (World Scientific Publishing Co Ltd, London, 1994), p. 2317. <https://doi.org/10.1142/2317>
14. S. Hamada, N. Burtebayev, N. Amangeldi et al., Phenomenological and semi-microscopic analysis for ^{16}O and ^{12}C elastically scattering on the nucleus of ^{16}O and ^{12}C at energies near coulomb barrier. *J. Phys. Conf. Ser.* **381**, 012130 (2012). <https://doi.org/10.1088/1742-6596/381/1/012130>
15. G. Bertsch, J. Borsowicz, H. McManus et al., Interactions for inelastic scattering derived from realistic potentials. *Nuclear Phys. A* **284**, 399–419 (1977). [https://doi.org/10.1016/0375-9474\(77\)90392-X](https://doi.org/10.1016/0375-9474(77)90392-X)
16. I. Gontcharn, D.J. Hinde, M. Dasgupta et al., Double folding nucleus-nucleus potential applied to heavy-ion fusion reactions. *Phys. Rev. C* **69**, 024610 (2004). <https://doi.org/10.1103/PhysRevC.69.024610>
17. S. Shlomo, D.H. Youngblood, Nuclear matter incompressibility and giant monopole resonance. *Nuclear Phys. A* **569**, 303–312 (1994). [https://doi.org/10.1016/0375-9474\(94\)90121-X](https://doi.org/10.1016/0375-9474(94)90121-X)
18. G. Colo, N.V. Giai, Theoretical understanding of the nuclear matter incompressibility: where do we stand? *Nuclear Phys. A* **731**, 15–27 (2004). <https://doi.org/10.1016/j.nuclphysa.2003.11.014>

19. K.C. Panda, B.C. Sahu, J. Bhoi, Accuracy of simple folding model in the calculation of the direct part of real $\alpha - \alpha$ interaction potential. *PRAMANA J. Phys.* **82**, 841–849 (2014). <https://doi.org/10.1007/s12043-014-0737-2>
20. L. Trache, A. Azhari, H.L. Clark et al., Optical model potential involving loosely bound p-shell nuclei around 10 MeV/nucleon. *Phys. Rev. C* **61**, 024612 (2000). <https://doi.org/10.1103/PhysRevC.61.024612>
21. F.A. Brieva, J.R. Rook, Nucleon-nucleus optical model (1). Nuclear matter approach. *Nuclear Phys. A* **291**, 299–316 (1977). [https://doi.org/10.1016/0375-9474\(77\)90322-0](https://doi.org/10.1016/0375-9474(77)90322-0)
22. E. Stiliaris, H.G. Bohlen, P. Frobrich et al., Nuclear rainbow structures in the elastic scattering of ^{16}O on ^{16}O at $E_{\text{Lab}} = 350$ MeV. *Phys. Lett. B* **223**, 291–295 (1989). [https://doi.org/10.1016/0370-2693\(89\)91604-3](https://doi.org/10.1016/0370-2693(89)91604-3)
23. H.G. Bohlen, E. Stiliaris, B. Gebauer et al., Refractive scattering and reactions, comparison of two systems: $^{16}\text{O} + ^{16}\text{O}$ and $^{20}\text{Ne} + ^{12}\text{C}$. *Z. Phys. A.* **346**, 189–200 (1993). <https://doi.org/10.1007/BF01306079>
24. G. Bartnitzky, A. Blazevic, H.G. Bohlen et al., Model-unrestricted nucleus-nucleus scattering potentials from measurement and analysis of $^{16}\text{O} + ^{16}\text{O}$ scattering. *Phys. Lett. B.* **365**, 23–28 (1996). [https://doi.org/10.1016/0370-2693\(95\)01292-3](https://doi.org/10.1016/0370-2693(95)01292-3)
25. Y. Sugiyama, Y. Tomita, H. Ikezoe et al., Observation of airy oscillation for the $^{16}\text{O} + ^{16}\text{O}$ system at $E_{\text{Lab}} = 145$ MeV. *Phys. Lett. B.* **312**, 35–39 (1993). [https://doi.org/10.1016/0370-2693\(93\)90482-W](https://doi.org/10.1016/0370-2693(93)90482-W)
26. C.A. Bertulani, A. Gade, Nuclear astrophysics with radioactive beams. *Phys. Rep.* **485**, 195–259 (2010). <https://doi.org/10.1016/j.Physrep.2009.09.002>
27. L.H. Chien, D.T. Khoa, D.C. Cuong et al., Consistent mean-field description of the $^{12}\text{C} + ^{12}\text{C}$ optical potential at low energies and the astrophysical S-factor. *Phys. Rev. C* **98**, 064001 (2018). <https://doi.org/10.1103/PhysRevC.98.064001>
28. N.L. Anh, N.H. Phuc, D.T. Khoa et al., Folding model approach to the elastic $p + ^{12,13}\text{C}$ scattering at low energies and radiative capture $^{12,13}\text{C}(p, \gamma)$ reactions. *Nuclear Phys. A.* **1006**, 122078 (2021). <https://doi.org/10.1016/j.nuclphysa.2020.122078>